



Characterization of a long non-coding RNA *Pcdh17it* as a novel marker for immature pre-myelinating oligodendrocytes

Journal:	GLIA
Manuscript ID	GLIA-00133-2019.R2
Wiley - Manuscript type:	Original Research Article
Date Submitted by the Author:	n/a
Complete List of Authors:	Kasuga, Yusuke; University College London, Wolfson Institute for Biomedical Research Fudge, Alexander; University College London, Wolfson Institute for Biomedical Research Zhang, Yumeng; UCL, Wolfson Institute for Biomedical Research, University College London Li, Huiliang ; University College London, Wolfson Institute for Biomedical Research
Topics:	Oligodendrocytes, CNS myelin, Development
Techniques:	In situ hybridization, Histological techniques, Cellular and Developmental Neuroscience
Key Words:	oligodendrocyte, long non-coding RNA, immature oligodendrocyte, oligodendrocyte dynamics, Pcdh17it

SCHOLARONE™
Manuscripts

Characterization of a long non-coding RNA *Pcdh17it* as a novel marker for immature pre-myelinating oligodendrocytes

Running title: New marker for immature oligodendrocytes

Yusuke Kasuga^{1,2,3}, Alexander D Fudge¹, Yumeng Zhang¹ and Huiliang Li¹

¹ Wolfson Institute for Biomedical Research, University College London, London, WC1E 6BT UK

² Department of Life Sciences, Graduate School of Arts and Sciences, University of Tokyo, Tokyo, Japan

³ Present address: Laboratory for Neural Circuitry of Learning and Memory, RIKEN Center for Brain Science, Wako, Saitama 351-0198, Japan

Correspondence: huiliang.li@ucl.ac.uk

Conflict of Interest: The authors declare no conflict of interest.

Data Availability Statement: The data that support the findings of this study are available from the corresponding author upon reasonable request.

Acknowledgements

This work was funded by the Biotechnology and Biological Sciences Research Council (BB/L003236/1 and BB/S000844/1 to H.L.). We are grateful to Prof WD Richardson for encouragement, advice and comments on the manuscript, as well as to other WIBR colleagues for advice and discussion. We thank Michael Wegner (University of Erlangen, Germany) and Qing Richard Lu (Cincinnati Children's Hospital Medical Center, USA) for sharing with us anti-Sox10 antibody and *Olig2^{loxP}* mice respectively.

Total word count: 6,783. 6 figures, 5 supplementary figures, 1 supplementary table. (Abstract 128, Introduction 510, Materials and Methods 892, Results 1,693, Discussion 945, Figure legends 783, References 1,571)

Key words: oligodendrocyte, long non-coding RNA, *Pcdh17it*, immature oligodendrocyte, pre-myelinating oligodendrocyte, oligodendrocyte dynamics

Main points:

1. *Pcdh17it* specifically marks newly born immature oligodendrocytes (OLs)
2. *Pcdh17it* is an effective tool for studying OL dynamics in situ
3. *Pcdh17it* helps subdivide immature OLs into two distinct developmental stages, “small spidery” and “large spidery”

Abstract

OL precursor cells (OPs) proliferate and differentiate into oligodendrocytes (OLs) during postnatal development and into adulthood in the central nervous system (CNS). Following the initiation of differentiation, OPs give rise to immature, pre-myelinating OLs, which undergo further differentiation and mature into myelin-forming OLs. We identified an immature OL-specific long non-coding RNA, named *Pcdh17it*. Through co-localization analysis and morphological characterization of OLs, we found that *Pcdh17it* is a specific marker for newly born immature OLs in the developing and adult forebrain of mice, and we used this new marker to analyze OL generation over the lifespan of mice. *Pcdh17it* is an effective tool for monitoring newly born OLs in adult brain, allowing detailed study of the dynamics of differentiation of OPs into OLs in the normal and pathological CNS.

Introduction

In the mammalian central nervous system (CNS), the majority of oligodendrocytes (OLs) are generated from OL precursors (OPs) in the early postnatal period, e.g. in the first ~6 weeks of age in mice (Psachoulia, Jamen, Young, & Richardson, 2009; Young et al., 2013). A large population of OPs (about 5% of all neural cells) persists in the adult mouse CNS and OPs continue to proliferate and differentiate into mature OLs, at a steadily reducing rate, throughout adult life (Psachoulia et al., 2009; Richardson, Young, Tripathi, & McKenzie, 2011). Although the function of adult-born OLs is still unclear, recent data from different laboratories suggest that they might contribute to neural plasticity by myelinating previously unmyelinated axons, thereby changing or stabilizing neural circuit function (Makinodan, Rosen, Ito, & Corfas, 2012; Mangin, Li, Scafidi, & Gallo, 2012; McKenzie et al., 2014; Scholz, Klein, Behrens, & Johansen-Berg, 2009; Xiao et al., 2016).

Between OPs and mature OLs, there exists an intermediate stage(s) of “pre-myelinating” OLs (i.e. newly forming or immature OLs, imOLs), in which the OP marker platelet derived growth factor receptor-alpha (*Pdgfra*) is turned off and mRNAs encoding myelin structural proteins such as myelin basic protein (*Mbp*) and myelin OL glycoprotein (*Mog*) start to be expressed (Zhang et al., 2014). Myelin proteins and their mRNAs continue to be expressed throughout the life of OLs, so that pre-myelinating imOLs are difficult or impossible to distinguish from myelinating OLs on the basis of myelin gene expression alone. So far, several markers including O4 antigen (Kuhlmann-Krieg et al., 1988), inositol 1,4,5-trisphosphate receptor type 2 (*Itpr2*; Marques et al., 2016), ectonucleotide pyrophosphatase /phosphodiesterase 6 (*Enpp6*; Xiao et al., 2016), breast carcinoma amplified sequence 1 (*Bcas1*; Fard et al., 2017) have been used to label imOLs, but each marker has its limitations. O4 antigen-labelling is mainly used in vitro and *Itpr2* labels astrocytes as well as immature OLs, while *Enpp6* and *Bcas1* continue to be expressed in mature OLs. Therefore, to streamline research into OL developmental dynamics in vivo it is important to discover new gene products that can distinguish pre-myelinating imOLs from both myelinating OLs and OPs in tissue sections. In recent years, high-throughput technologies such as transcriptome profiling, single-cell sequencing and proteomics have helped build informative databases covering OL lineage cells (Cahoy et al., 2008; Zhang et al., 2014; Sharma et al., 2015; Marques et al., 2016; Marques et al., 2018;). Here, tapping into available data, we identify an OL lineage-specific long non-coding RNA (lncRNA; Zhang et al., 2014) that is down-regulated in myelinating OLs and provide evidence that this lncRNA (named *Pcdh17it*) is a specific marker for immature, pre-myelinating imOLs. This lncRNA has previously been named *9630013A20Rik* (Zeisel et al., 2015), *IncOL1* (He et al., 2017) and *Pcdh17it* (Marques et al., 2017), and we adopt the name *Pcdh17it* in accord with the guidelines of the

HUGO Gene Nomenclature Committee (Wright, 2014). In addition, we show that *Pcdh17it* expressing cells in adult mouse brain are newly generated cells and, with the help of this new marker, we demonstrate OL generation over the lifespan in mouse forebrain.

Results

***Pcdh17it* expression in immature OLs in postnatal developing forebrain**

In our search for genes expressed specifically in imOLs, we analyzed an RNA-seq database of mouse brain cells (Zhang et al., 2014) and found that expression of lncRNA *9630013A20Rik* (called *Pcdh17it*) is at high levels in newly formed OLs (NFOLs) but at much lower levels in myelinating OLs and OPs (**Fig. 1A**). Furthermore, *Pcdh17it* expression is absent from astrocytes, neurons, microglia and endothelial cells. Therefore, *Pcdh17it* appeared to be a promising candidate marker for imOLs.

We first examined *Pcdh17it* expression in mouse forebrain by RNA in situ hybridization (ISH) at postnatal day 14 (P14) and found that *Pcdh17it* was expressed in the nucleus and/or cytoplasm of certain cells (**Fig. 1B-D**). We next analyzed cellular co-localization of *Pcdh17it* with OL lineage- and stage-specific markers in mouse forebrain. In both subcortical white matter and cerebral cortex, almost all *Pcdh17it*⁺ cells co-expressed Sox10 and Olig2 (**Fig. 1E, F** and **Fig. S1A, B**), two well-known OL lineage-specific transcription factors (Kuhlbrodt, Herbarth, Sock, Hermans-Borgmeyer, & Wegner, 1998; Lu et al., 2000; Zhou, Wang, & Anderson, 2000), indicating that *Pcdh17it* specifically marks OL lineage cells. At the same time, only a small minority of *Pcdh17it*⁺ cells expressed *Pdgfra* mRNA, a marker of OPs (Pringle, Mudhar, Collarini, & Richardson, 1992) (**Fig. 1G** and **Fig. S1C**), suggesting that the great majority of *Pcdh17it*⁺ cells are not OPs. CC1 is an antibody against adenomatous polyposis coli (*Apc*), often used for labelling the cell bodies of differentiated OLs (Bhat et al., 1996; Xiao et al., 2016). Approximately 60% of *Pcdh17it*⁺ cells were CC1⁺ (**Fig. 1H** and **Fig. S1D**) and about 65% of *Pcdh17it*⁺ cells co-expressed *Mbp* mRNA (**Fig. 1I**), a marker of immature and mature OLs (Xiao et al., 2016). Taken together, these data reveal *Pcdh17it* expression in OL lineage cells in P14 developing mouse brain and suggest that most *Pcdh17it*-expressing cells are at a transitional stage between *Pdgfra*⁺ OPs and CC1⁺ or *Mbp*⁺ differentiated OLs.

Given that Olig2 is essential to OL development (Lu et al., 2002; Zhou & Anderson, 2002), to further verify the identity of *Pcdh17it*⁺ cells, we examined *Pcdh17it* expression in the forebrain of P14 *Sox10-Cre: Olig2^{loxP/loxP}* mice (cKO) with *Sox10-Cre:Olig2^{loxP/+}* mice as controls (Ctrl). We found that the substantial loss of Olig2⁺ cells in cKO mice compared to controls [cKO vs Ctrl: 261.60 ± 36.72 vs 4017.00 ± 49.71 cells/mm² (mean ± SEM), *p*<0.001, 5 animals per group] was mirrored by a significant drop in the number of *Pcdh17it*⁺ cells (cKO vs Ctrl: 43.33 ± 2.27 vs 181.40 ± 4.29 cells/mm², *p*<0.001; **Fig. S1E, F**). In addition, we observed minimal or no co-expression of *Pcdh17it* with markers for neurons (NeuN;

Fig. S2A, B), astrocytes [fibroblast growth factor receptor 3 (*Fgfr3*) and glial fibrillary acidic protein (*Gfap*); **Fig. S2C, D**] or neural stem cells (*Gfap* and *Ki67*; **Fig. S2D, E**). Taken together, these data are in favour of *Pcdh17it* as a specific marker of imOLs.

Combining *Pcdh17it* expression with morphological characterization of OLs

It has been suggested that morphological characterization of cells expressing *Mbp* or myelin proteolipid protein (Plp) can help differentiate ‘pre-myelinating’ OLs from mature OLs in rodent and human brain (Chang, Nishiyama, Peterson, Prineas, & Trapp, 2000; Trapp, Nishiyama, Cheng, & Macklin, 1997; Xiao et al., 2016). For *Mbp* (mRNA)-expressing OLs, those with a distinct ‘spidery’ morphology are likely to be newly forming pre-myelinating OLs, whereas those with smaller, weakly stained “non-spidery” cell bodies/soma are likely to be mature OLs that provide myelin sheaths for nearby axons (Xiao et al., 2016). Hence, we examined the morphology of *Mbp*- and *Pcdh17it*- expressing OLs in cerebral cortex of P14 mice. As in the previous study (Xiao et al., 2016), we found *Mbp*-expressing OLs with ‘spidery’ radial processes (**Fig. 2B-D**). When combined with *Mbp* protein immunolabelling, we could further divide *Mbp*⁺ spidery OLs into two subtypes – *Mbp*⁺/*Mbp*⁻ ‘small-spidery’ OLs and *Mbp*⁺/*Mbp*⁺ ‘large-spidery’ OLs, with mean radii of arborizing processes $25.29 \pm 2.11 \mu\text{m}$ versus $64.78 \pm 3.49 \mu\text{m}$, respectively (mean \pm SEM; $n=36$ and 122 cells; $p<0.001$; cells measured in 3 sections from 3 mice; **Fig. 2B, C, F, G**). Notably, all small-spidery cells expressed *Pcdh17it* but not *Mbp* protein (i.e. 100% of them were *Pcdh17it*⁺/*Mbp*⁺/*Mbp*⁻, $n=36$, 3 sections from 3 mice). In contrast, all large-spidery cells displayed *Mbp* immunoreactivity but most were *Pcdh17it*-negative (i.e. 66% of large-spidery cells were *Pcdh17it*⁻/*Mbp*⁺/*Mbp*⁺ and 34% were *Pcdh17it*⁺/*Mbp*⁺/*Mbp*⁺; $n=122$; 3 sections from 3 mice; **Fig. 2B, C, E**). *Pcdh17it* was not detected in *Mbp*⁺/*Mbp*⁺ non-spidery OLs, indicating that *Pcdh17it* is not expressed in mature myelinating OLs (**Fig. 2D, E**).

From these results and taking into account the fact that *Pcdh17it* was found in a small number of *Pdgfra*⁺ OPs (**Fig. 1G**), the most likely developmental sequence is as follows: 1) *Pdgfra*⁺, *Mbp*⁻, *Pcdh17it*⁻ OPs exit the cell cycle to become *Pdgfra*⁺, *Mbp*⁻, *Pcdh17it*⁺ post-mitotic OPs, 2) they lose *Pdgfra* and acquire *Mbp* mRNA expression to become *Pdgfra*⁻, *Mbp*⁺/*Mbp*⁻, *Pcdh17it*⁺ small-spidery pre-myelinating imOLs, 3) they progress to *Mbp*⁺/*Mbp*⁺, *Pcdh17it*⁺ then *Mbp*⁺/*Mbp*⁺, *Pcdh17it*⁻ large-spidery imOLs (**Fig. 2A-C, E**), 4) they mature into *Mbp*⁺/*Mbp*⁺, *Pcdh17it*⁻ non-spidery myelinating OLs. Together, these results support the proposition that *Pcdh17it* is a specific marker of pre-myelinating imOLs, between dividing OPs and fully mature, myelinating OLs and help distinguish two developmental subtypes of imOLs.

***Pcdh17it* expression in immature OLs in adult forebrain**

OL generation occurs not only during early postnatal development but also in adulthood (Rivers et al., 2008; Dimou et al., 2008; Young et al., 2013). To find out if *Pcdh17it* expression can define imOLs in adult brain, we also carried out co-localization analyses of *Pcdh17it* with OL stage-specific markers in the forebrain of P75 mice. Similar to the pattern in P14 forebrain, only a small number of *Pcdh17it*⁺ cells co-expressed *Pdgfra* in the subcortical white matter and cerebral cortex (**Fig. 3A, B**), while 50-60% of them were positive for CC1 and *Mbp* mRNA (**Fig. 3C-F**). These data, consistent with the results obtained from P14 developing brain, reveal *Pcdh17it*-expressing OLs in adult mouse brain and suggest that they represent an early stage of OL differentiation.

***Pcdh17it* as a specific marker for newly-formed immature OLs in adult brain**

To determine whether *Pcdh17it*⁺ OLs are newly formed imOLs in adult brain, we used 5-ethynyl-2'-deoxyuridine (EdU, a nucleoside analog to thymidine) to label dividing cells, almost all of which are OPs in adult brain (Rivers et al., 2008; Young et al., 2013), and examined *Pcdh17it* expression in EdU⁺ progeny cells. EdU was administered to mice at P60 for 37 or 52 days via their drinking water and forebrain tissue was collected at P97 or P112 (**Fig. 4A**). In subcortical white matter, all *Pcdh17it*-expressing cells were positive for EdU at both P97 and P112 (**Fig. 4B-C**), proving that *Pcdh17it*⁺ cells are newly born cells. In addition, all *Pcdh17it*⁺ cells were Ki67 negative (**Fig. S2E** and data not shown), so they were not actively dividing. Therefore, these data point to *Pcdh17it* as a specific marker for newly formed imOLs in adult mouse brain.

OL lineage dynamics over the lifetime in mouse forebrain

During CNS development, *Pdgfra*⁺ OPs appear in the medial ganglionic eminence (MGE) in the ventral forebrain at embryonic day 12.5 (E12.5) and cortically-derived OPs can be observed from E18.5 in mouse brain (Richardson, Kessaris, & Pringle, 2006); around 10 days after birth, *Mbp*⁺ mature OLs start to be seen, particularly in corpus callosum (Fyffe-Maricich, Karlo, Landreth, & Miller, 2011; Giera et al., 2015). OPs are able to proliferate and produce mature OLs into adulthood (McKenzie et al., 2014; Xiao et al., 2016; Young et al., 2013). Although it is becoming clear that OL generation continues throughout life with significant implications for brain function and plasticity, the dynamics of OL lineage cells over the lifetime have not yet been well characterized. To this end, we examined density dynamics of different types of OL lineage cells in mouse forebrain using OL stage-specific markers including *Pdgfra* for OPs, *Pcdh17it* for imOLs, *Enpp6* and *Mbp* for immature/mature OLs. At E15.5, only *Pdgfra*⁺ OPs could be seen scattered unevenly in different regions of

the forebrain, while *Pcdh17it⁺* imOLs and *Enpp6^{high}* or *Mbp⁺* immature/mature OLs were not found (**Table S1** and data not shown). The same situation was found on the day of birth (postnatal day zero, P0) (data not shown, **Fig. 5** and **Table S1**). The density of *Pdgfra⁺* OPs rose sharply to a peak between P0 to P7, then decreased gradually with increasing age until it levelled off after P75-P100 (**Figs. 5, S3, S4** and **Table S1**). *Pcdh17it⁺* imOLs were first widely detected on P7 and increased in number thereafter until P14 [or P30 in the cingulate area (CA)] before declining gradually with age. The rise and fall of *Pcdh17it⁺* imOLs was approximately mirrored by *Enpp6^{high}* imOLs (**Figs. 5, S3, S4** and **Table S1**). *Mbp⁺* immature/ mature OLs first appeared on P7 and their numbers increased after that, the rate of increase slowing after P75 and almost, but not quite, flattening out after P100 (**Figs. 5, S3, S4** and **Table S1**), consistent with earlier findings (Tripathi et al., 2017). In addition, OL lineage dynamics in different forebrain regions were in sync over the lifespan except for a delay in the peak of pre-myelinating imOLs in the CA (**Fig. 5**). It is worth mentioning that *Pcdh17it⁺* imOLs were first detected at E15.5 in mouse ventral spinal cord (data not shown), consistent with the early onset of OP differentiation in spinal cord.

These data demonstrate: 1) OPs are the predominant type of OL lineage cells in neonatal developing brain, 2) OPs' differentiation rate peaks at P14 (or P30 in CA), 3) following the near-completion of OL development 2-3 months after birth, the production of mature OLs by OPs shifts to a lower gear in young adult brain after ~P100; 4) OPs are able to continue generating new mature OLs (via imOLs) in adult brain at a slow rate, and this ability declines with increasing age, 5) overall, OL generation in different forebrain regions (apart from CA) seems to proceed according to the same clock across the lifespan.

Materials and Methods

Animals

Sox10-Cre:Olig2^{loxP/loxP} mice were generated by breeding *Sox10-Cre* mice (Matsuoka et al., 2005) to *Olig2^{loxP/loxP}* conditional knockout mice (Cai et al., 2007). C57/B6 mice were purchased from Charles River Laboratories. Mouse husbandry and all procedures were carried out in accordance with UK Home Office regulations, UCL Ethics Committee guidelines and the UK Animals (Scientific Procedures) Act 1986 and its Amendment Regulations (2012).

Tissue preparation

Mice of different ages (P7-P330) were subjected to intra-cardiac perfusion with cold 4% (w/v) paraformaldehyde (PFA; Sigma) in diethylpyrocarbonate (DEPC)-treated phosphate-buffered saline (PBS) under terminal anaesthesia, then brain tissues were immediately

dissected and post-fixed in 4% PFA at 4°C for 24 hours. E15.5 and P0 mice were decapitated and brain tissues immediately immersion-fixed with cold 4% (w/v) PFA at 4°C overnight. The tissues were then cryoprotected in 20% (w/v) sucrose (Sigma) overnight before being embedded in Tissue-Tek® OCT (VWR) on dry ice for rapid freezing. Frozen coronal forebrain sections (20µm) were cut with a cryostat, mounted on Superfrost® Plus slides (VWR) and air-dried for at least 2 hours at 20-25°C before use.

***Pcdh17it* ISH probe design**

Six *Pcdh17it* transcript variants of different sizes have been reported (Carninci & Hayashizaki, 1999; Carninci et al., 1996; Katayama et al., 2005; Kawai et al., 2001; Okazaki et al., 2002; Shibata et al., 2000). We designed a riboprobe specific to a sequence shared by all variants produced from the last exon of the *Pcdh17it* gene. The DNA template corresponding to a 1,400 bp segment in exon 6 of *9630013A20Rik* was acquired by PCR with a pair of primers, probe-F: 5'-ACAGGTGTGCTCCTCATAAGTG-3' and probe-R: 5'-TAATACGACTCACTATAGGGCTTTGCTGTGACTTACACAGC-3' (T7 promoter sequence underlined).

RNA *in situ* hybridization (ISH)

Our ISH protocol has been described previously (Pringle et al., 2003). Briefly, digoxigenin (DIG)- or fluorescein isothiocyanate (FITC)-labelled riboprobes were synthesized *in vitro* using DNA templates of mouse *Pcdh17it* (DIG/FITC), *Pdgfra* (FITC), *Mbp* (FITC) and *Enpp6* (DIG) (Pringle et al., 2003; Xiao et al., 2016). For single chromogenic RNA ISH, hybridization products were visualized using alkaline phosphatase (AP)-conjugated anti-DIG or anti-FITC antibody with a mixture of nitroblue tetrazolium (NBT) and 5-bromo-4-chloro-3-indolyl phosphate (toluidine salt, BCIP; all reagents from Roche). When detecting *Enpp6*, the colour was allowed to develop until we could detect *Enpp6*^{high} newly-forming OLs, but not *Enpp6*^{low} mature OLs (Xiao et al., 2016). For double fluorescence RNA ISH, two probes, one labelled with FITC and the other with DIG, were applied to sections simultaneously for overnight hybridization. FITC and DIG were detected sequentially with horseradish peroxidase (HRP)-conjugated anti-FITC antibody followed by HRP-conjugated anti-DIG and the signal was developed using the TSA Plus FITC/Cyanine 3 (Cy3) kit following the manufacturer's instructions (Perkin Elmer). Before DIG detection, 3% (w/v) H₂O₂ was used to inactivate the FITC-conjugated HRP.

RNA ISH combined with immunostaining

We used our published protocol for combining fluorescence RNA ISH with immunolabelling (Jolly, Fudge, Pringle, Richardson, & Li, 2016). In brief, following single or double fluorescence RNA ISH (described above), immunolabelling was performed as follows: tissue sections were incubated with blocking buffer [10% (v/v) heat-inactivated sheep serum in PBS] and then with rabbit anti-Olig2 (1:400; Millipore ab9610), guinea pig anti-Sox10 (1:2,000; gift from M. Wegner), mouse CC1 (1:200; Millipore op80), rat anti-Mbp (1:200; Abcam ab89780), mouse anti-NeuN (1:500; Millipore mab377), rabbit anti-Gfap (1:2,000; Dako Z0334) or mouse anti-Ki67 (1:10; BD Pharmingen 550609) primary antibody overnight (over 3 days for rat anti-Mbp) at 4°C. For Olig2, NeuN, Gfap and Ki67 immunolabelling, Alexa Fluor 488-, 568- or 647-conjugated secondary antibody was used (1:750; Thermo Fisher Scientific). For Sox10, CC1 and Mbp immunolabelling, following incubation with H₂O₂ to quench HRP, sections were incubated with biotin-conjugated donkey anti-rabbit/rat/mouse/guinea pig secondary antibody (1:200; Thermo Fisher Scientific) followed by incubation with a mix of VECTASTAIN ABC solutions A and B (Vector Laboratories) for 40 minutes at 20-25°C and reaction product was visualized using the TSA Plus FITC, Cy3 or Cy5 kit.

Cell counting and measurement

For co-localization analyses, low-magnification (20x objective) and high-magnification (60x objective) images of corpus callosum and motor cortex between the dorsolateral corners of the lateral ventricles were collected from three or more mice using a Leica TCS SP5 confocal microscope with LAS AF LITE software. Images were captured as Z stacks with 0.5µm spacing using standard excitation and emission filters and exported into ImageJ to create 'orthogonal views' (where cells do not vertically overlap along the Z stack of images) for cell counting. 40-300 cells were counted for each data point. Image J was also used for measuring the radii of the process fields of 'large/small spidery' OLs.

To analyze OL lineage dynamics in different regions across mouse forebrain, bright field images of whole sections (20 µm thickness) were captured using a Zeiss Axio Scan Z.1 slide scanner with ZEN2 software, which was used for calculation of cell number-density. Cell numbers were counted within the whole region under study.

***In vivo* EdU labelling**

EdU was administrated to mice in their drinking water (0.2 mg/ml) for 37 days or 52 days from P60. At P97 or P112, forebrain tissues were collected and prepared as described

above. After *Pcdh17it* RNA ISH, EdU was detected using the Alexa Fluor 555 Click-iT kit (Invitrogen).

Statistics

The cell counts, OL process radii and cell density data were analyzed statistically using GraphPad Prism 5 software, with which the mean, SEM and *p*-value of unpaired two-tailed *t*-tests were calculated. $p < 0.05$ was considered statistically significant.

Discussion

***Pcdh17it* as a specific marker for immature OLs**

Through co-localization analyses and EdU incorporation assays, we showed that *Pcdh17it* is a specific marker for newly forming imOLs in developing and adult forebrain in mice (**Fig. 6**). Compared to two recently reported imOL markers *Enpp6* (Xiao et al., 2016) and *Bcas1* (Fard et al., 2017), *Pcdh17it* expression seems to better align with an intermediate stage between OPs and mature OLs, hence providing higher specificity for imOLs (**Figs. 1, 3, 6, S1, and S5A-D**). *Enpp6* is also weakly expressed in mature OLs with high levels of co-localization (~90%) with CC1, and *Bcas1* was also detected in some mature OLs, agreeing with data from a recently published single cell RNA-seq database for OL lineage cells (Marques et al., 2016; Marques et al., 2018; **Fig. S5C-D**). This database categorizes gene expression into 13 different OL subtype/ developmental stage clusters (**Fig. S5A**) and reveals that *Pcdh17it* expression is elevated in two clusters of newly-formed imOLs while *Enpp6* and *Bcas1* expression is scattered in numerous clusters of OL subtypes/ stages (**Fig. S5B-D**). We limited the colour development time in RNA ISH of *Enpp6* to allow detection of only *Enpp6*^{high} imOLs (**Figs. 5, S3, S4**; Xiao et al., 2016).

Pdgfra protein expression is exclusive to OPs, but because currently available anti-*Pdgfra* antibodies do not work well after RNA ISH, we used double RNA ISH to examine co-localization of *Pdgfra* and *Pcdh17it* RNA. We detected a small population of *Pdgfra*⁺/*Pcdh17it*⁺ double-positive cells, which might correspond to a transitional phase from OP to imOL, warranting further investigation in respect of *Pcdh17it* function.

CC1 has been broadly used for labelling mature OLs and is considered to be an antibody against adenomatous polyposis coli (*Apc*; Bhat et al., 1996). However, *Apc* is predominantly expressed in neurons and only transiently expressed in OL lineage cells during OL development and remyelination (Lang et al., 2013). Some evidence even suggests that CC1 does not bind to *Apc* but to RNA binding protein Quaking 7 (*Qki-7*), which is up-regulated in myelinating OLs (Bin, Harris, & Kennedy, 2016; Lang et al., 2013). Despite disagreement about the target of CC1, our previous study suggests that CC1 can label mature OLs and also late stage imOLs (Xiao et al., 2016). In addition to CC1 co-localization, our conclusion that *Pcdh17it* is not expressed in mature OLs is also built on morphological features and its lack of co-expression with *Mbp* protein (Trapp et al., 1997; Xiao et al., 2016; **Fig. 2**).

Our data reveal that “small spidery” and “large spidery” imOLs differ not only in size, but also in *Pcdh17it* expression, hinting at two distinct stages of imOLs. A likely developmental sequence is: post-mitotic OPs → “small spidery” imOLs → “large spidery” imOLs → “non-

spidery" mature OLs. Progress along this sequence might be controlled by signals, including activity-dependent signals, from unmyelinated axons.

The biology of immature OLs

Recent studies show by in vivo two-photon imaging that mature myelinating OLs are long-lived (Hill, Li, & Grutzendler, 2018; Hughes, Orthmann-Murphy, Langseth, & Bergles, 2018), and the same conclusion was also reached by population-based analyses in transgenic reporter mice (Tripathi et al., 2017). However, little is known about the stability and survival time of pre-myelinating imOLs. We were unable to study apoptosis of *Pcdh17it⁺* imOLs by anti-Caspase-3 immunolabelling because the immunoreactivity of cleaved Caspase-3 did not survive RNA-ISH.

Given the specificity of *Pcdh17it* expression for imOLs, its promoter might be useful for generating transgenic reporter mice for future studies of imOLs in the developing, adult and diseased CNS. It will be interesting, for example, to discover whether imOLs are all destined to differentiate into mature OLs or whether they have other functions in their own right.

Potential function of *Pcdh17it* in immature OLs

lncRNAs are extremely abundant, with ~60,000 different lncRNA species in human (Iyer et al., 2015). lncRNAs are generally expressed at low levels, in relatively short time windows and with selective tissue specificity. Most lncRNAs are located in the nucleus where they regulate gene expression near or away from their sites of synthesis through cis- or trans-acting mechanisms (Postepska-Igielska et al., 2015). A small proportion of lncRNAs reside in the cytoplasm where they likely regulate protein trafficking, mRNA translation and stability (Rashid, Shah, & Shan, 2016). We provide evidence that *Pcdh17it* is specifically expressed in imOLs and is present in both cytoplasm and/or nucleus (**Fig. 1**). *Pcdh17it* (also known as *9630013A20Rik* or *IncOL1*) was reported to regulate OL differentiation through interaction with polycomb repressive complex 2 (Prc2) via Suz12 (He et al., 2017). The *Pcdh17it* gene lies inside intron 1 of the *Pcdh17* gene (encoding cell-cell adhesion molecule Protocadherin 17), in the antisense direction, on mouse chromosome 14. During neuronal development, Pcdh17 of neurons forms intercellular homophilic interactions via its extracellular domain and recruits actin polymerization regulators such as the WAVE regulatory complex via its cytoplasmic domain, thereby directing axons to extend together in fascicles (Hoshina et al., 2013). Interestingly, for myelination, the initiation of OL process extension and axon ensheathment requires polymerization of f-actin, whereas subsequent myelin wrapping requires disassembly of f-actin (Zuchero et al., 2015). It has been shown that *Wave1/ Wsf1* knockout in mice leads to fewer OL processes per cell and hypomyelination in the white

matter (Kim et al., 2006). Despite the fact that no significant correlation was found between *Pcdh17* and *Pcdh17it* expression by an earlier bioinformatics analysis (He et al., 2017), we discovered that they are largely co-expressed in imOLs (**Fig. S5E, F**; A. Fudge and H. Li unpublished observations). Taken together, the available evidence suggests that that *Pcdh17* might take part in the initiation of myelination by regulating f-actin assembly while *Pcdh17it* might fine-tune the level of *Pcdh17* expression.

References

- Bhat, R.V., Axt, K.J., Fosnaugh, J.S., Smith, K.J., Johnson, K.A., Hill, D.E., . . . Baraban, J.M. (1996). Expression of the APC tumor suppressor protein in oligodendroglia. *Glia* 17, 169-174. doi:10.1002/(SICI)1098-1136(199606)17:2<169::AID-GLIA8>3.0.CO;2-Y
- Bin, J.M., Harris, S.N., & Kennedy, T.E. (2016). The oligodendrocyte-specific antibody 'CC1' binds Quaking 7. *J Neurochem* 139, 181-186. doi:10.1111/jnc.13745
- Cahoy, J.D., Emery, B., Kaushal, A., Foo, L.C., Zamanian, J.L., Christopherson, K.S., . . . Barres, B.A. (2008). A transcriptome database for astrocytes, neurons, and oligodendrocytes: a new resource for understanding brain development and function. *J Neurosci* 28, 264-278. doi:10.1523/JNEUROSCI.4178-07.2008
- Cai, J., Chen, Y., Cai, W.H., Hurlock, E.C., Wu, H., Kernie, S.G., . . . Lu, Q.R. (2007). A crucial role for Olig2 in white matter astrocyte development. *Development* 134, 1887-1899. doi:10.1242/dev.02847
- Carninci, P., & Hayashizaki, Y. (1999). High-efficiency full-length cDNA cloning. *Methods Enzymol* 303, 19-44.
- Carninci, P., Kvam, C., Kitamura, A., Ohsumi, T., Okazaki, Y., Itoh, M., . . . Schneider, C. (1996). High-efficiency full-length cDNA cloning by biotinylated CAP trapper. *Genomics* 37, 327-336. doi:10.1006/geno.1996.0567
- Chang, A., Nishiyama, A., Peterson, J., Prineas, J., & Trapp, B.D. (2000). NG2-positive oligodendrocyte progenitor cells in adult human brain and multiple sclerosis lesions. *J Neurosci* 20, 6404-6412.
- Fard, M.K., van der Meer, F., Sanchez, P., Cantuti-Castelvetri, L., Mandad, S., Jakel, S., . . . Simons, M. (2017). BCAS1 expression defines a population of early myelinating oligodendrocytes in multiple sclerosis lesions. *Sci Transl Med* 9. doi:10.1126/scitranslmed.aam7816
- Fyffe-Maricich, S.L., Karlo, J.C., Landreth, G.E., & Miller, R.H. (2011). The ERK2 mitogen-activated protein kinase regulates the timing of oligodendrocyte differentiation. *J Neurosci* 31, 843-850. doi:10.1523/JNEUROSCI.3239-10.2011
- Giera, S., Deng, Y., Luo, R., Ackerman, S.D., Mogha, A., Monk, K.R., . . . Piao, X. (2015). The adhesion G protein-coupled receptor GPR56 is a cell-autonomous regulator of oligodendrocyte development. *Nat Commun* 6, 6121. doi:10.1038/ncomms7121
- He, D., Wang, J., Lu, Y., Deng, Y., Zhao, C., Xu, L., . . . Lu, Q.R. (2017). lncRNA functional networks in oligodendrocytes reveal stage-specific myelination control by an lncOL1/Suz12 complex in the CNS. *Neuron* 93, 362-378. doi:10.1016/j.neuron.2016.11.044
- Hill, R.A., Li, A.M., & Grutzendler, J. (2018). Lifelong cortical myelin plasticity and age-related degeneration in the live mammalian brain. *Nat Neurosci* 21, 683-695. doi:10.1038/s41593-018-0120-6
- Hoshina, N., Tanimura, A., Yamasaki, M., Inoue, T., Fukabori, R., Kuroda, T., . . . Yamamoto, T. (2013). Protocadherin 17 regulates presynaptic assembly in

- topographic corticobasal Ganglia circuits. *Neuron* 78, 839-854. doi:10.1016/j.neuron.2013.03.031
- Hughes, E.G., Orthmann-Murphy, J.L., Langseth, A.J., & Bergles, D.E. (2018). Myelin remodeling through experience-dependent oligodendrogenesis in the adult somatosensory cortex. *Nat Neurosci* 21, 696-706. doi:10.1038/s41593-018-0121-5
- Iyer, M.K., Niknafs, Y.S., Malik, R., Singhal, U., Sahu, A., Hosono, Y., . . . Chinnaiyan, A.M. (2015). The landscape of long noncoding RNAs in the human transcriptome. *Nat Genet* 47, 199-208. doi:10.1038/ng.3192
- Jolly, S., Fudge, A., Pringle, N., Richardson, W.D., & Li, H. (2016). Combining double fluorescence in situ hybridization with immunolabelling for detection of the expression of three genes in mouse brain sections. *J Vis Exp* (109), e53976. doi:10.3791/53976
- Katayama, S., Tomaru, Y., Kasukawa, T., Waki, K., Nakanishi, M., Nakamura, M., . . . Consortium, F. (2005). Antisense transcription in the mammalian transcriptome. *Science* 309, 1564-1566. doi:10.1126/science.1112009
- Kawai, J., Shinagawa, A., Shibata, K., Yoshino, M., Itoh, M., Ishii, Y., . . . the, F. C. (2001). Functional annotation of a full-length mouse cDNA collection. *Nature* 409, 685-690. doi:10.1038/35055500
- Kim, H.J., DiBernardo, A.B., Sloane, J.A., Rasband, M.N., Solomon, D., Kosaras, B., . . . Vartanian, T.K. (2006). WAVE1 is required for oligodendrocyte morphogenesis and normal CNS myelination. *J Neurosci* 26, 5849-5859. doi:10.1523/JNEUROSCI.4921-05.2006
- Kuhlbrodt, K., Herbarth, B., Sock, E., Hermans-Borgmeyer, I., & Wegner, M. (1998). Sox10, a novel transcriptional modulator in glial cells. *J Neurosci* 18, 237-250.
- Kuhlmann-Krieg, S., Sommer, I., & Schachner, M. (1988). Ultrastructural features of cultured oligodendrocytes expressing stage-specific cell-surface antigens. *Brain Res* 467, 269-280.
- Lang, J., Maeda, Y., Bannerman, P., Xu, J., Horiuchi, M., Pleasure, D., & Guo, F. (2013). Adenomatous polyposis coli regulates oligodendroglial development. *J Neurosci* 33, 3113-3130. doi:10.1523/JNEUROSCI.3467-12.2013
- Lu, Q.R., Sun, T., Zhu, Z., Ma, N., Garcia, M., Stiles, C. D., & Rowitch, D.H. (2002). Common developmental requirement for Olig function indicates a motor neuron/oligodendrocyte connection. *Cell* 109, 75-86.
- Lu, Q.R., Yuk, D., Alberta, J.A., Zhu, Z., Pawlitzky, I., Chan, J., . . . Rowitch, D.H. (2000). Sonic hedgehog--regulated oligodendrocyte lineage genes encoding bHLH proteins in the mammalian central nervous system. *Neuron* 25, 317-329.
- Makinodan, M., Rosen, K.M., Ito, S., & Corfas, G. (2012). A critical period for social experience-dependent oligodendrocyte maturation and myelination. *Science* 337, 1357-1360. doi:10.1126/science.1220845
- Mangin, J.M., Li, P., Scafidi, J., & Gallo, V. (2012). Experience-dependent regulation of NG2 progenitors in the developing barrel cortex. *Nat Neurosci* 15, 1192-1194. doi:10.1038/nn.3190

- Marques, S., van Bruggen, D., Vanichkina, D.P., Floriddia, E.M., Munguba, H., Varemo, L., . . . Castelo-Branco, G. (2018). Transcriptional convergence of oligodendrocyte lineage progenitors during development. *Dev Cell* 46, 504-517 e507. doi:10.1016/j.devcel.2018.07.005
- Marques, S., Vanichkina, D., van Bruggen, D., Floriddia, E. M., Munguba, H., Väre, L., . . . Castelo-Branco, G. (2017). Single-cell transcriptomic profiling of progenitors of the oligodendrocyte lineage reveals transcriptional convergence during development. *bioRxiv* 186445. doi:10.1101/186445
- Marques, S., Zeisel, A., Codeluppi, S., van Bruggen, D., Mendanha Falcao, A., Xiao, L., . . . Castelo-Branco, G. (2016). Oligodendrocyte heterogeneity in the mouse juvenile and adult central nervous system. *Science* 352, 1326-1329. doi:10.1126/science.aaf6463
- Matsuoka, T., Ahlberg, P.E., Kessar, N., Iannarelli, P., Dennehy, U., Richardson, W.D., . . . Koentges, G. (2005). Neural crest origins of the neck and shoulder. *Nature* 436, 347-355. doi:10.1038/nature03837
- McKenzie, I.A., Ohayon, D., Li, H., de Faria, J.P., Emery, B., Tohyama, K., & Richardson, W.D. (2014). Motor skill learning requires active central myelination. *Science* 346, 318-322. doi:10.1126/science.1254960
- Okazaki, Y., Furuno, M., Kasukawa, T., Adachi, J., Bono, H., Kondo, S., . . . Team, I. I. (2002). Analysis of the mouse transcriptome based on functional annotation of 60,770 full-length cDNAs. *Nature* 420, 563-573. doi:10.1038/nature01266
- Postepska-Igielska, A., Giwojna, A., Gasri-Plotnitsky, L., Schmitt, N., Dold, A., Ginsberg, D., & Grummt, I. (2015). LncRNA Khps1 regulates expression of the proto-oncogene SPHK1 via triplex-mediated changes in chromatin structure. *Mol Cell* 60, 626-636. doi:10.1016/j.molcel.2015.10.001
- Pringle, N.P., Mudhar, H.S., Collarini, E.J., & Richardson, W.D. (1992). PDGF receptors in the rat CNS: during late neurogenesis, PDGF alpha-receptor expression appears to be restricted to glial cells of the oligodendrocyte lineage. *Development* 115, 535-551.
- Pringle, N.P., Yu, W.-P., Howell, M., Colvin, J.S., Ornitz, D. M., & Richardson, W.D. (2003). Fgfr3 expression by astrocytes and their precursors: evidence that astrocytes and oligodendrocytes originate in distinct neuroepithelial domains. *Development* 130, 93-102.
- Psachoulia, K., Jamen, F., Young, K.M., & Richardson, W.D. (2009). Cell cycle dynamics of NG2 cells in the postnatal and ageing brain. *Neuron Glia Biol* 5, 57-67. doi:10.1017/S1740925X09990354
- Rashid, F., Shah, A., & Shan, G. (2016). Long Non-coding RNAs in the Cytoplasm. *Genomics Proteomics Bioinformatics* 14, 73-80. doi:10.1016/j.gpb.2016.03.005
- Richardson, W.D., Kessar, N., & Pringle, N. (2006). Oligodendrocyte wars. *Nat Rev Neurosci* 7, 11-18. doi:10.1038/nrn1826
- Richardson, W.D., Young, K.M., Tripathi, R.B., & McKenzie, I. (2011). NG2-glia as multipotent neural stem cells: fact or fantasy? *Neuron* 70, 661-673. doi:10.1016/j.neuron.2011.05.013

- Rivers, L.E., Young, K.M., Rizzi, M., Jamen, F., Psachoulia, K., Wade, A., Kessarar, N. and Richardson, W.D. (2008). PDGFRA/NG2-positive glia generate myelinating oligodendrocytes and piriform projection neurons in adult mice. *Nat. Neurosci.* **11**, 1392-1401.
- Scholz, J., Klein, M.C., Behrens, T.E., & Johansen-Berg, H. (2009). Training induces changes in white-matter architecture. *Nat Neurosci*, **12**(11), 1370-1371. doi:10.1038/nn.2412
- Sharma, K., Schmitt, S., Bergner, C.G., Tyanova, S., Kannaiyan, N., Manrique-Hoyos, N., . . . Simons, M. (2015). Cell type- and brain region-resolved mouse brain proteome. *Nat Neurosci* **18**, 1819-1831. doi:10.1038/nn.4160
- Shibata, K., Itoh, M., Aizawa, K., Nagaoka, S., Sasaki, N., Carninci, P., . . . Togawa, Y. (2000). RIKEN integrated sequence analysis (RISA) system--384-format sequencing pipeline with 384 multicapillary sequencer. *Genome Res* **10**, 1757-1771.
- Trapp, B.D., Nishiyama, A., Cheng, D., & Macklin, W. (1997). Differentiation and death of premyelinating oligodendrocytes in developing rodent brain. *J Cell Biol* **137**, 459-468.
- Tripathi, R.B., Jackiewicz, M., McKenzie, I.A., Kougioumtzidou, E., Grist, M., & Richardson, W.D. (2017). Remarkable stability of myelinating oligodendrocytes in mice. *Cell Rep* **21**, 316-323. doi:10.1016/j.celrep.2017.09.050
- Wright, M. W. (2014). A short guide to long non-coding RNA gene nomenclature. *Hum Genomics* **8**, 7. doi:10.1186/1479-7364-8-7
- Xiao, L., Ohayon, D., McKenzie, I.A., Sinclair-Wilson, A., Wright, J.L., Fudge, A.D., . . . Richardson, W.D. (2016). Rapid production of new oligodendrocytes is required in the earliest stages of motor-skill learning. *Nat Neurosci* **19**, 1210-1217. doi:10.1038/nn.4351
- Young, K.M., Psachoulia, K., Tripathi, R.B., Dunn, S.J., Cossell, L., Attwell, D., . . . Richardson, W.D. (2013). Oligodendrocyte dynamics in the healthy adult CNS: evidence for myelin remodeling. *Neuron* **77**, 873-885. doi:10.1016/j.neuron.2013.01.006
- Zhang, Y., Chen, K., Sloan, S.A., Bennett, M.L., Scholze, A.R., O'Keeffe, S., . . . Wu, J.Q. (2014). An RNA-sequencing transcriptome and splicing database of glia, neurons, and vascular cells of the cerebral cortex. *J Neurosci* **34**, 11929-11947. doi:10.1523/JNEUROSCI.1860-14.2014
- Zhou, Q., & Anderson, D.J. (2002). The bHLH transcription factors OLIG2 and OLIG1 couple neuronal and glial subtype specification. *Cell* **109**, 61-73.
- Zhou, Q., Wang, S., & Anderson, D. J. (2000). Identification of a novel family of oligodendrocyte lineage-specific basic helix-loop-helix transcription factors. *Neuron* **25**, 331-343.
- Zuchero, J.B., Fu, M.M., Sloan, S.A., Ibrahim, A., Olson, A., Zaremba, A., . . . Barres, B.A. (2015). CNS myelin wrapping is driven by actin disassembly. *Dev Cell* **34**, 152-167. doi:10.1016/j.devcel.2015.06.011

Zeisel, A., Munoz-Manchado, A.B., Codeluppi, S., Lonnerberg, P., La Manno, G., Jureus, A., . . . Linnarsson, S. (2015). Brain structure. Cell types in the mouse cortex and hippocampus revealed by single-cell RNA-seq. *Science*, 347(6226), 1138-1142. doi:10.1126/science.aaa1934

Figure Legends

Fig. 1. Analysis of *Pcdh17it* expression in mouse forebrain at P14. (A) Expression of *Pcdh17it* (9630013A20Rik) in neural cells based on analysis of RNA-seq data (Zhang et al., 2014). (B-D) Detection of *Pcdh17it* expression (green) in cytoplasm (B), nucleus (C) and both nucleus and cytoplasm (D) of cells in P14 mouse forebrain by fluorescence RNA ISH. The nucleus was counter-stained with Hoechst dye (Hch, blue). (E-I) Co-localization of *Pcdh17it* with OL developmental stage-specific markers. Representative images are shown of cells labelled red for *Pcdh17it* (E-I) and green for Sox10 (E), Olig2 (F), *Pdgfra* (G), CC1 (H), or *Mbp* (I) in subcortical white matter of P14 mice. Cells that are double-labelled (arrows) or that express *Pcdh17it* alone (arrowheads) are indicated. A double-labelled cell (asterisked arrow) is shown at higher magnification at the right (E-I), aligned with z-stack images to the right (vertical) and below (horizontal). Each bar diagram to the left denotes the percentage of cells expressing one or two markers (mean \pm SEM; data from at least 4 mice). Note that a large fraction of CC1⁺ OLs in P14 brain are by definition recently generated and newly-myelinating, since OL differentiation in forebrain does not start until around the time of birth. Scale bars: 10 μ m (B-D); 30 μ m (E-I) and 10 μ m for high magnification images (E-I).

Fig. 2. Combining *Pcdh17it* expression with morphological characterization of OLs in cerebral cortex of P14 mice. (A-D) Cells expressing *Pcdh17it* (blue), *Mbp* (green) and *Mbp* (red) were labelled by double ISH followed by immunolabeling for *Mbp* in forebrain sections. (A) A *Pcdh17it*^{+/+}/*Mbp*^{-/-}/*Mbp*⁻ OP/ imOL, (B) a *Pcdh17it*^{+/+}/*Mbp*^{+/+}/*Mbp*⁻ “small spidery” imOL, (C) a *Pcdh17it*^{+/+}/*Mbp*^{+/+}/*Mbp*⁺ “large spidery” imOL, (D) a *Pcdh17it*^{+/+}/*Mbp*^{+/+}/*Mbp*⁺ “non-spidery” mature OL. Z-stack images to the right (vertical) and below (horizontal) are aligned with each image. Scale bars, 20 μ m. (E) A bar diagram illustrates percentages of cells expressing one, two and three markers (data from 3 mice; mean \pm SEM). (F) Reconstructed images of a *Mbp*^{+/+}/*Mbp*⁻ “small spidery” imOL and a *Mbp*^{+/+}/*Mbp*⁺ “large spidery” imOL. Each red circle is expanded by 10 μ m in radius drawn to scale with ImageJ. (G) Graph of the mean (\pm SEM) radius of arborizing processes of *Mbp*^{+/+}/*Mbp*⁻ “small spidery” imOLs (n=36) compared to *Mbp*^{+/+}/*Mbp*⁺ “large spidery” imOLs (n=122; data from 3 mice; ****p*<0.001 for unpaired *t*-test).

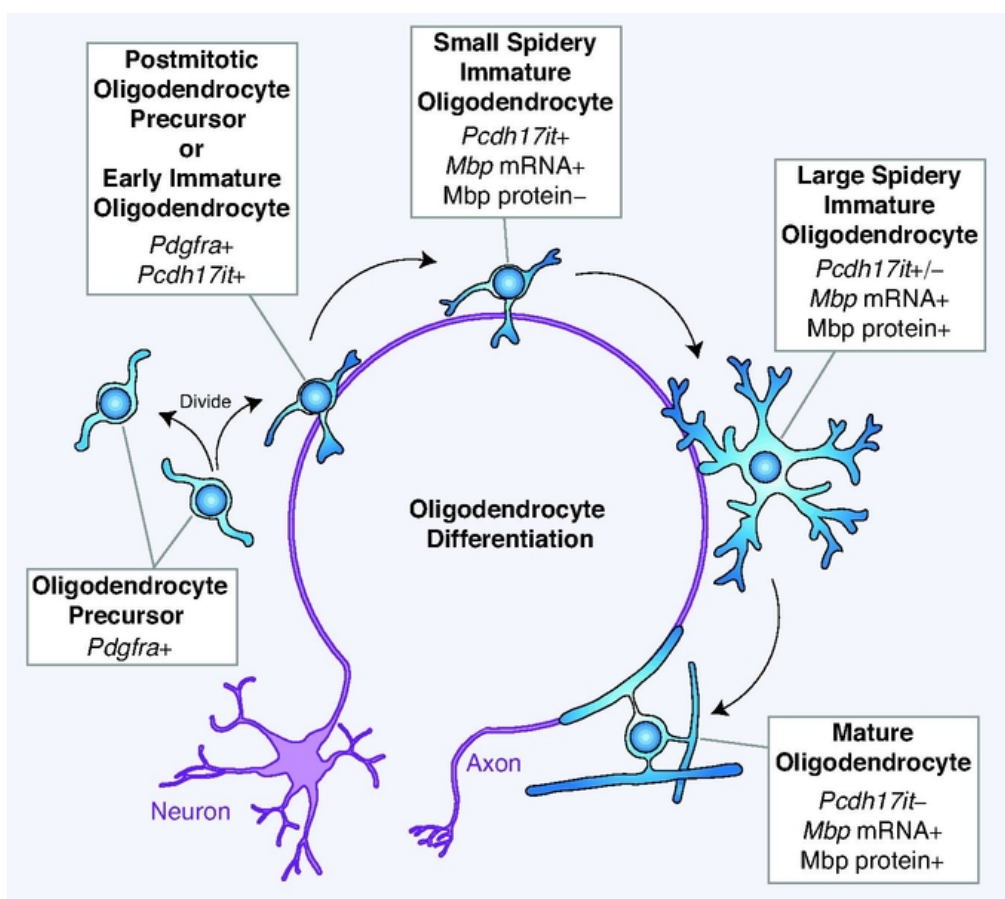
Fig. 3. Co-localization of *Pcdh17it* with OL stage-specific markers in the forebrain of P75 mice. (A-F) Cells labelled red for *Pcdh17it* (A-F) and green for *Pdgfra* (A, B), CC1 (C, D) or *Mbp* (E-F) in corpus callosum (A, C, E) and motor cortex (B, D, F). Cell nuclei were counter-stained with Hoechst dye (blue). Double-labelled cells (arrows) and cells expressing

Pcdh17it alone (arrowheads) are indicated. The bar diagram to the right of each image denotes percentages of cells expressing one and two markers (mean \pm SEM; data from at least 4 mice). Scale bars, 30 μ m.

Fig. 4. *Pcdh17it*-expressing OLs are newly born cells in adult brain. (A) Timeline of EdU administration. P60 mice were given EdU in their drinking water for 37 or 52 days before being sacrificed for *Pcdh17it* ISH and EdU staining in brain sections. (B, C) Cells labelled for EdU (red) and *Pcdh17it* (green) in corpus callosum at P97 (B) and P112 (C). Nuclei were counter-stained blue with Hoechst dye. All *Pcdh17it*⁺ cells were also EdU⁺. EdU⁺/*Pcdh17it*⁺ cells and EdU⁺-only cells are indicated by arrows and arrowheads respectively. Data from 3 mice for each time point. Scale bars, 10 μ m.

Fig. 5. Dynamics of OL lineage cells in mouse forebrain over the lifetime (P0 to P330). (A) Illustration of forebrain coronal section depicting structural regions (colours corresponding to regions in B). (B) Graphs showing cell densities of *Pdgfra*⁺, *Pcdh17it*⁺, *Enpp6*^{high} and *Mbp*⁺ OL lineage cells over the lifetime in different forebrain regions (* p <0.01, ** p <0.05, *** p <0.001 for unpaired *t*-tests). */**/** statistical significance is aligned with the older of any two adjacent ages compared. P0 to P75: n=6, P100/ P330: n=4.

Fig. 6. OL lineage progression and expression of stage-specific markers. Proteins are in plain font, RNAs are in italics. *Olig2* and *Sox10* are expressed through all stages of OL lineage progression. *Pdgfra* is expressed in OPs and is down-regulated while *Pcdh17it* expression is up-regulated at the initiation of OP differentiation. Later, *Pcdh17it*⁺ imOLs express *Mbp* and then CC1 antigen. In the final stages of OL differentiation, *Pcdh17it* expression is down-regulated while *Mbp* protein starts to be expressed. *Enpp6* expression starts at a high level in imOLs and persists at a lower level in mature OLs. *Bcas1* is expressed in imOLs but is also detectable in some mature OLs. By comparison, *Pcdh17it* expression is specific to imOLs.



TOCI

57x50mm (300 x 300 DPI)

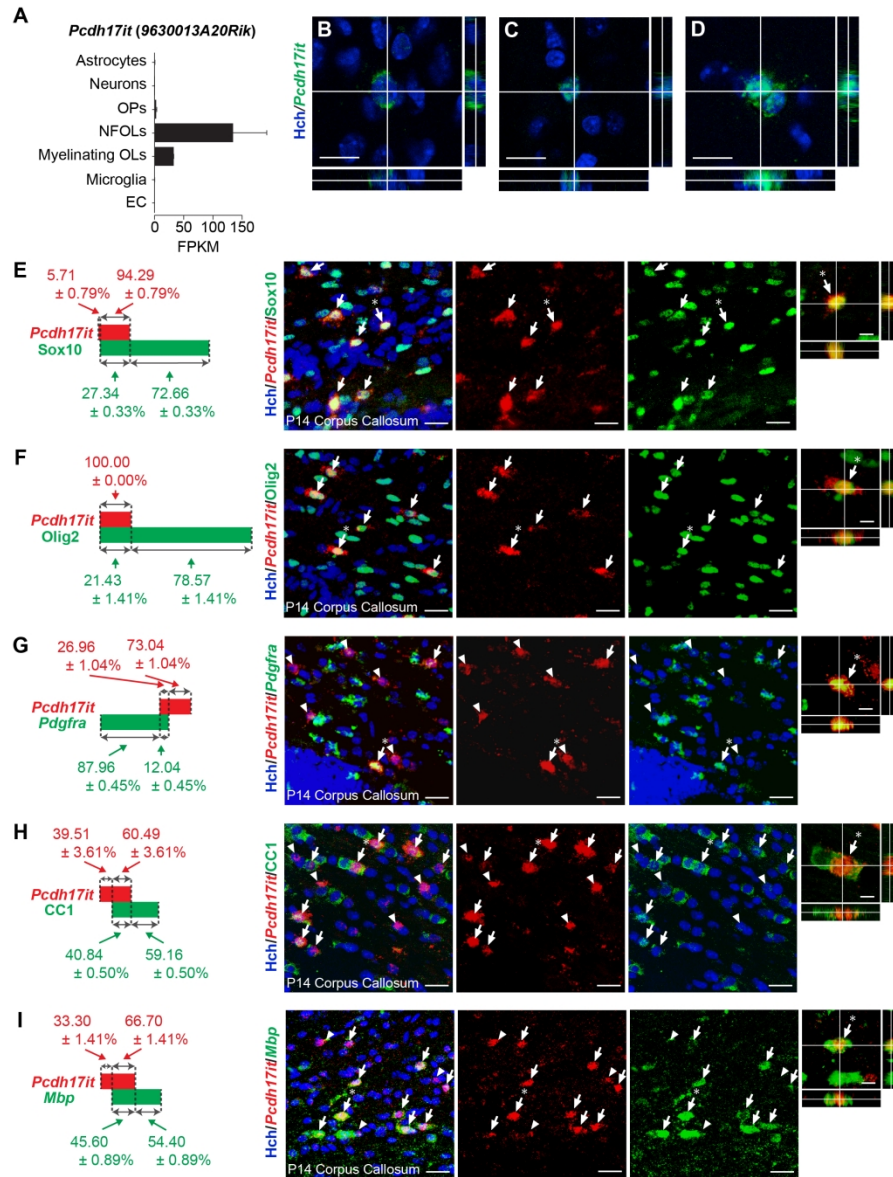


Fig. 1. Analysis of *Pcdh17it* expression in mouse forebrain at P14.

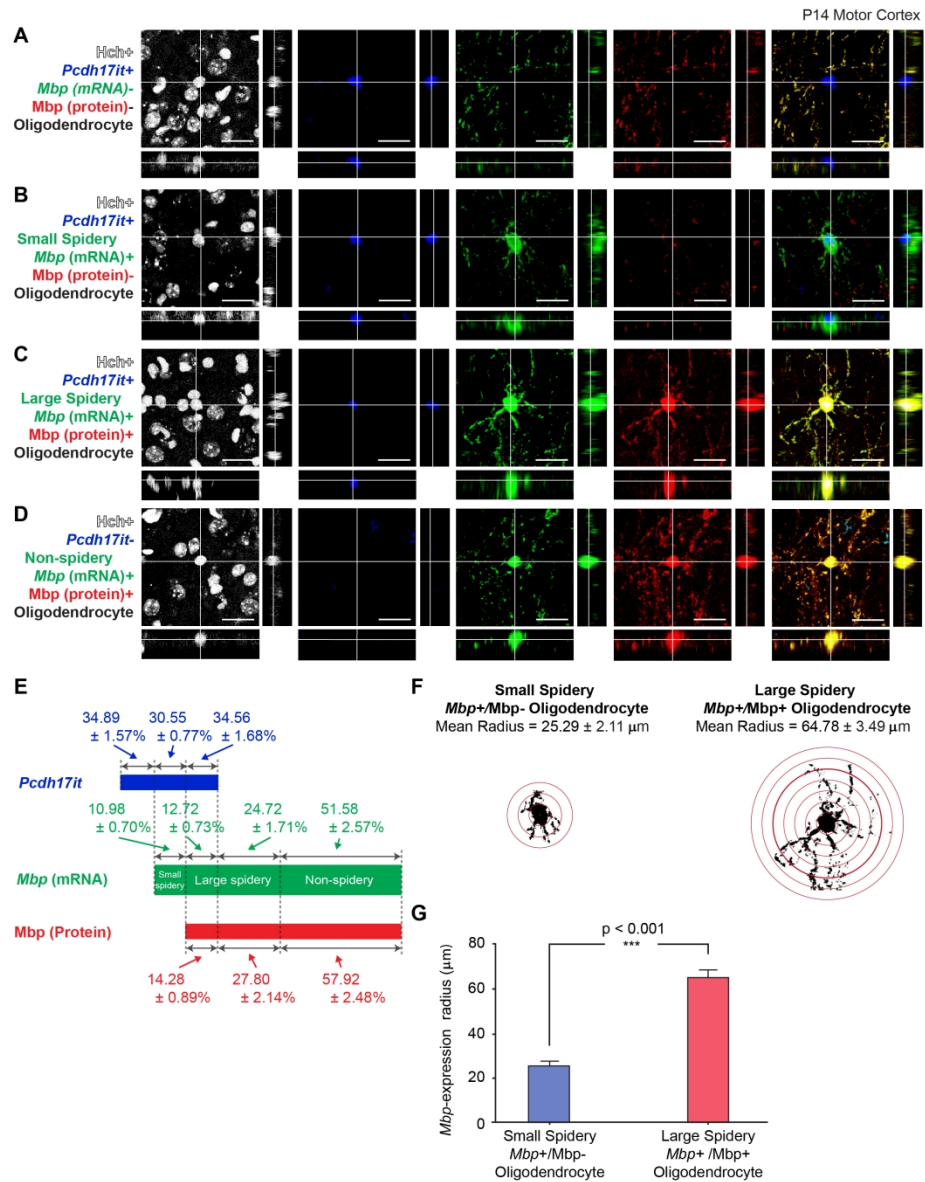


Fig. 2. Combining Pcdh17it expression with morphological characterization of OLs in cerebral cortex of P14 mice.

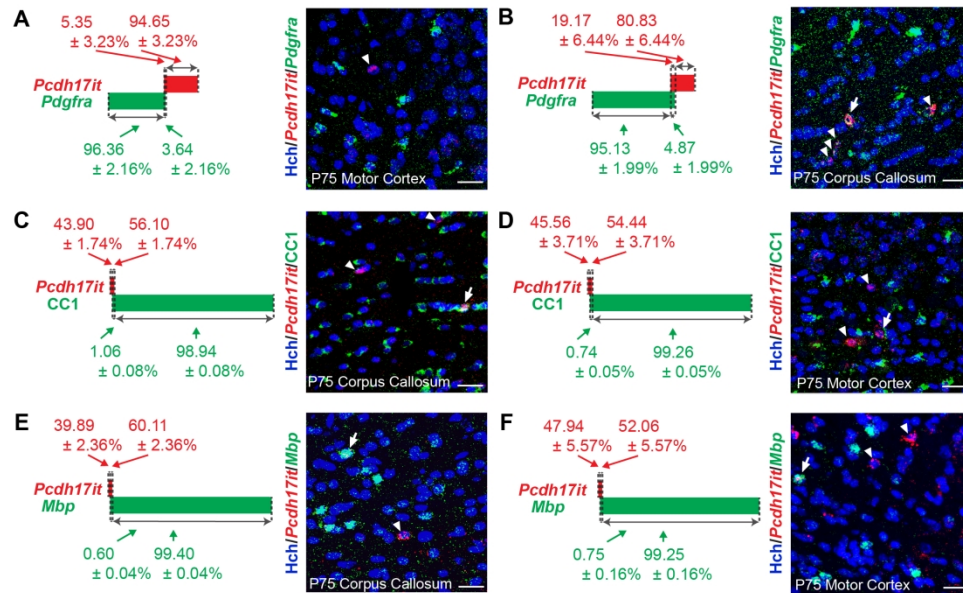


Fig. 3. Co-localization of *Pcdh17it* with OL stage-specific markers in the forebrain of P75 mice.

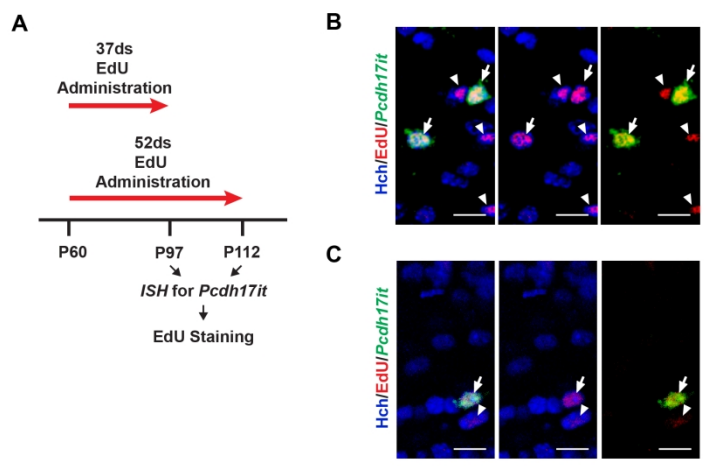


Fig. 4. *Pcdh17it*-expressing OLS are newly born cells in adult brain.

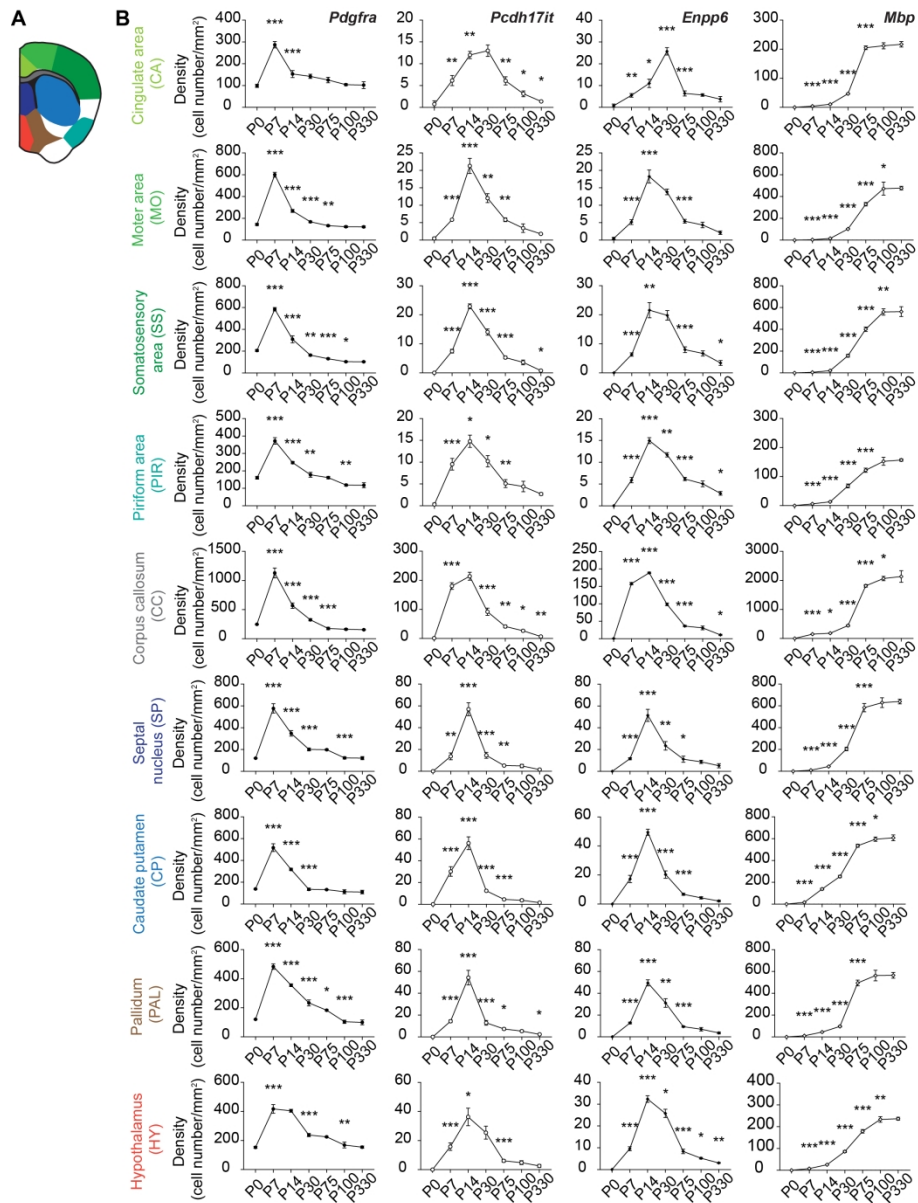


Fig. 5. Dynamics of OL lineage cells in mouse forebrain over the lifetime (P0 to P330).

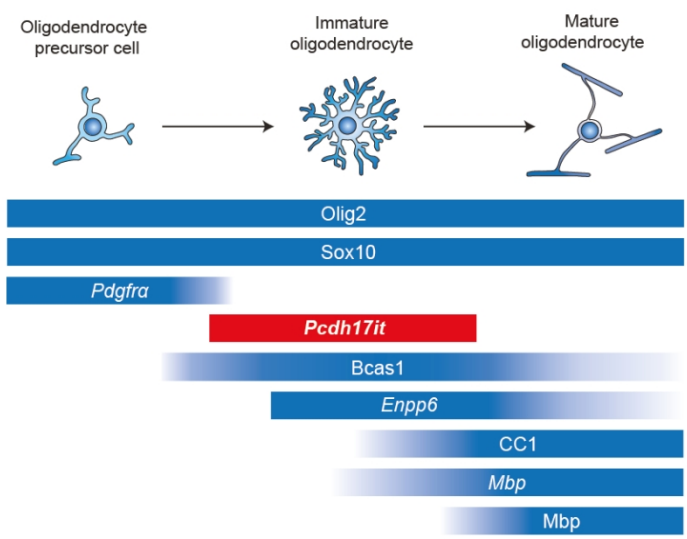


Fig. 6. OL lineage progression and expression of stage-specific markers.

Supplementary information

Supplementary Fig. 1. Identity of *Pcdh17it*-expressing cells. (A-D) Co-localization of *Pcdh17it* with OL developmental stage-specific markers in cerebral cortex of P14 mice. Cells labelled red for *Pcdh17it* (A-D) and green for Sox10 (A), Olig2 (B), *Pdgfra* (C), or CC1 (D) are shown. Cell nuclei were counter-stained blue with Hoechst dye. Arrows and arrowheads indicate double-labelled cells and cells expressing *Pcdh17it* alone, respectively. The bar diagrams to the left of each image denote percentages of cells that express one or two markers (mean \pm SEM; data from at least 4 mice). Scale bars: 30 μ m. (E, F) *Pcdh17it* expression in P14 *Olig2* cKO mice. (E) Cells expressing Olig2 (red) and *Pcdh17it*(green) in the forebrain of *Olig2* cKO and control mice. CC: corpus callosum, CCX: cerebral cortex. Scale bars, 50 μ m. (F) Graphs showing significant reductions in the density of Olig2⁺ (left) and *Pcdh17it*⁺ (right) cells in subcortical white matter (WM) in *Olig2* cKO mice compared to controls (mean \pm SEM; *** p <0.001 for unpaired t-tests). Data from 5 cKO mice and 5 controls.

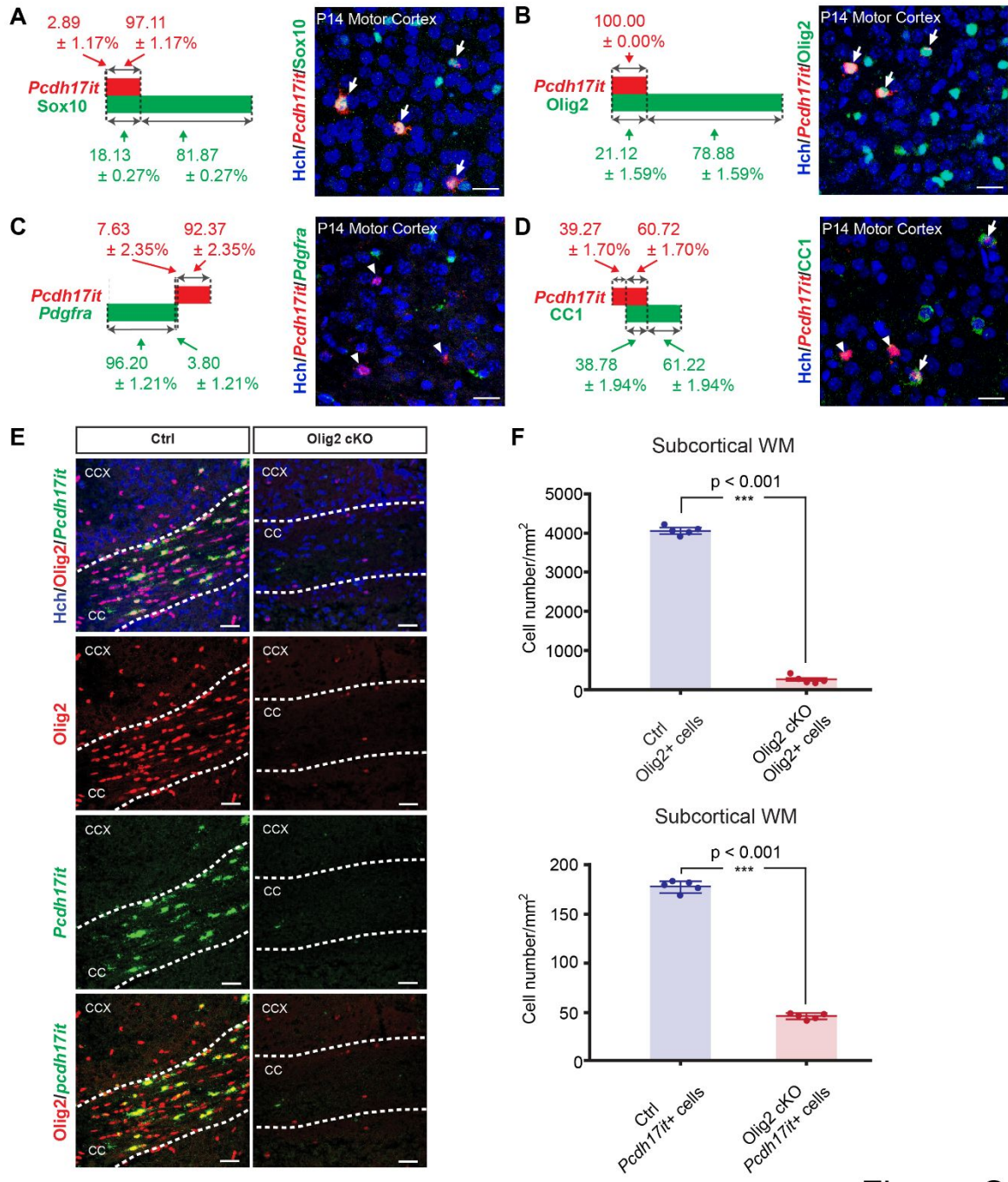
Supplementary Fig. 2. Co-localization of *Pcdh17it* with markers for neurons (NeuN), astrocytes (*Fgfr3* and *Gfap*) or neural stem cells (Ki67 and *Gfap*) in the forebrain of P14 mice. (A-E) Cells expressing *Pcdh17it* (red, A-E) and co-labelled (green) for NeuN (A, B), *Fgfr3* (C), *Gfap* (D) or Ki67 (E). The bar diagram to the right (A) shows percentages of *Pcdh17it*⁺, NeuN⁺ double-labelled cells in motor cortex. No other co-localization was observed (B-E). Arrowheads point at *Pcdh17it*⁺ cells. Data from at least 4 mice. CC: corpus callosum, SVZ: subventricular zone, LV: lateral ventricle. Scale bars: 30 μ m.

Supplementary Fig. 3. Expression of OL stage-specific markers in cortical regions of mouse forebrain at different ages (from P7 to P330). RNA ISH images of *Pdgfra*, *Pcdh17it*, *Enpp6*^{high} and *Mbp* expression in different cortical regions. Scale bars, 150 μ m. CA: cingulate area. MO: motor area. SS: somatosensory area. PIR: piriform area. CC: corpus callosum. CP: caudate putamen.

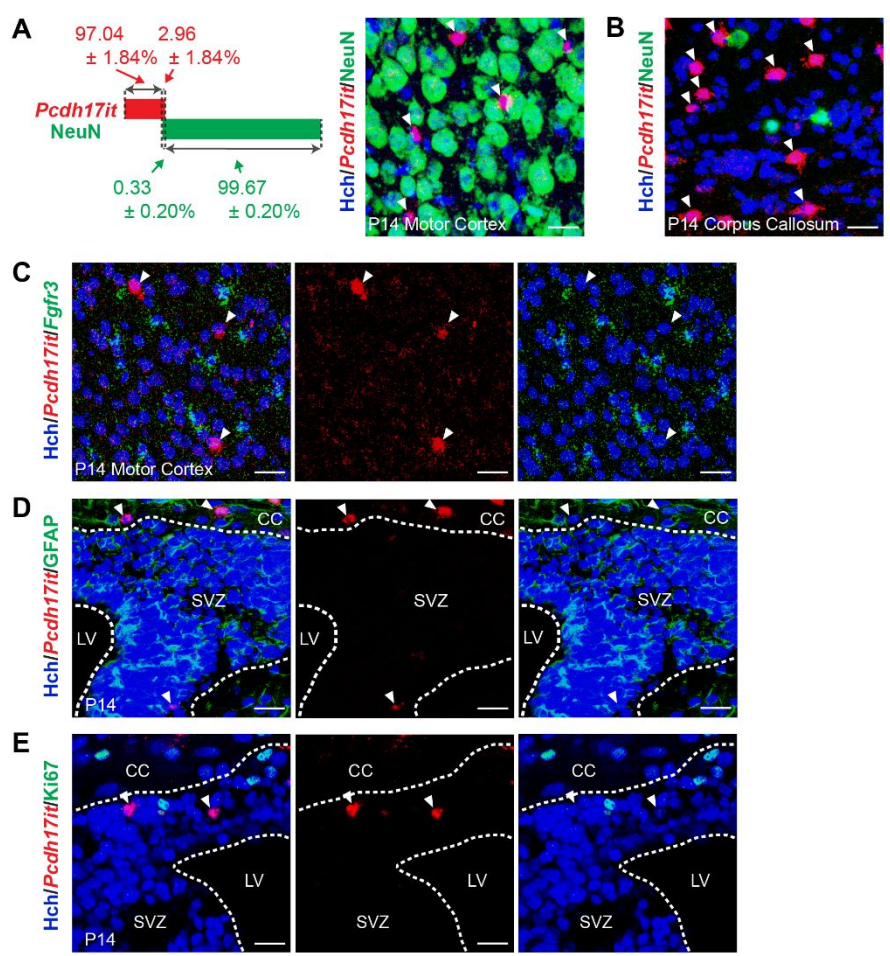
Supplementary Fig. 4. Expression of OL stage-specific markers in non-cortical regions of mouse forebrain at different ages (from P7 to P330). RNA ISH images of *Pdgfra*, *Pcdh17it*, *Enpp6*^{high} and *Mbp* expression in non-cortical regions of forebrain. Scale bars, 150 μ m. CA: cingulate area. cing: cingulum. MO: motor area. SP: septal nucleus. CC: corpus callosum. CP: caudate putamen. LV: lateral ventricle. SS: somatosensory area. PAL: pallidum. HY: hypothalamus.

Supplementary Fig. 5. Gene expression in OL lineage cells of a series of progression stages based on analysis of single-cell RNA-seq data. (A) Clustering pattern of OL lineage cells expressing mRNAs of 13 different OL subtypes/ developmental stages on the t-distributed stochastic neighbour embedding (t-SNE) trajectory map from OPs to mature OLs (**adapted from** Fig. 2A of Marques et al., 2016). (B-E) Plotted expression patterns on t-SNE trajectory map (left) and average expression levels (right) of *Pcdh17it* (B), *Enpp6*^{high} (C), *Bcas1* (D) and *Pcdh17* (E). (F) A Photoshop overlaid image of expression trajectories of *Pcdh17it* (green) and (red) from OPs to mature OLs. Simultaneous expression of *Pcdh17it* and *Pcdh17* in newly-formed imOLs (NFOLs) can be observed.

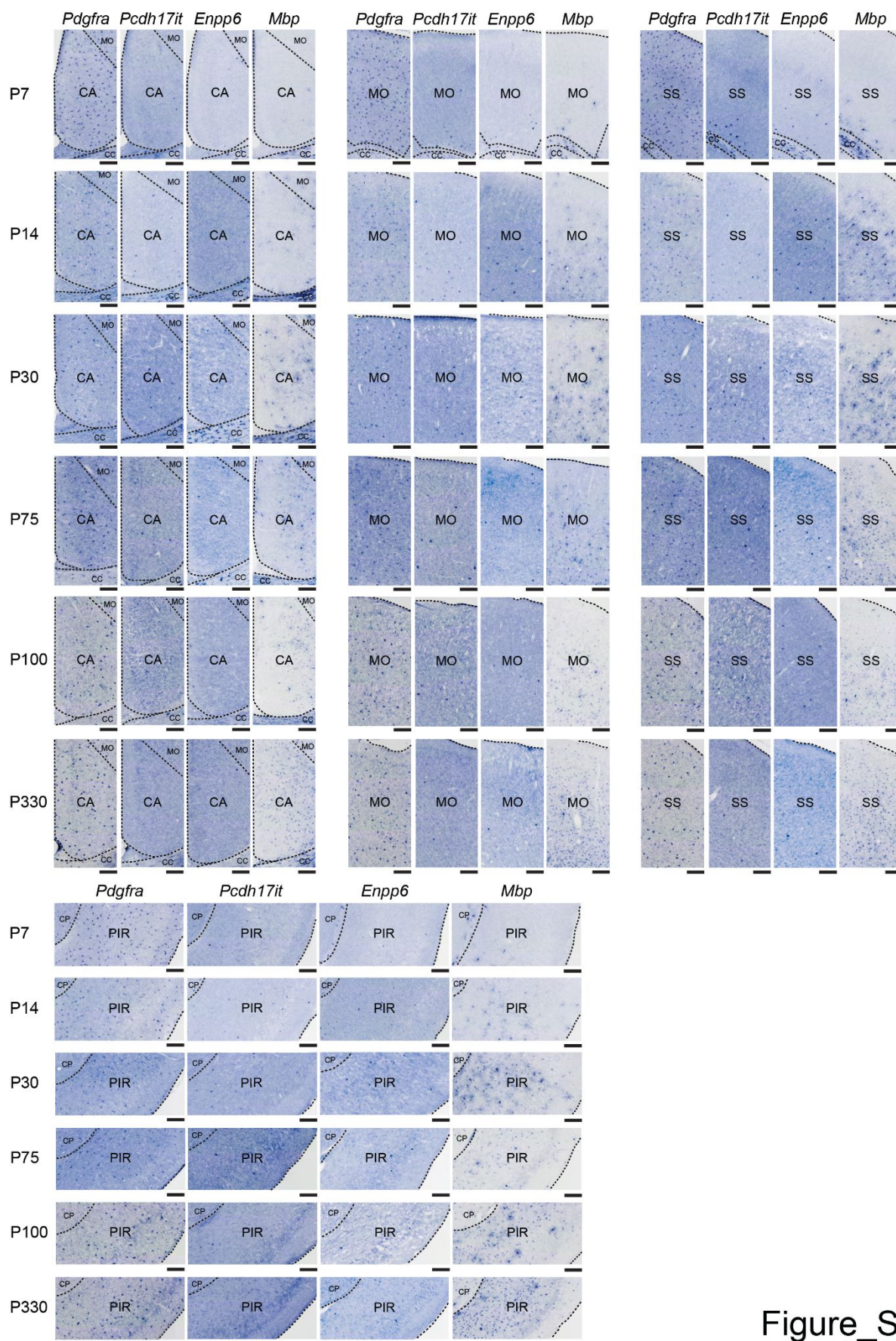
Supplementary Table 1. Number-densities of OL lineage cells in various regions of mouse forebrain over the lifetime.



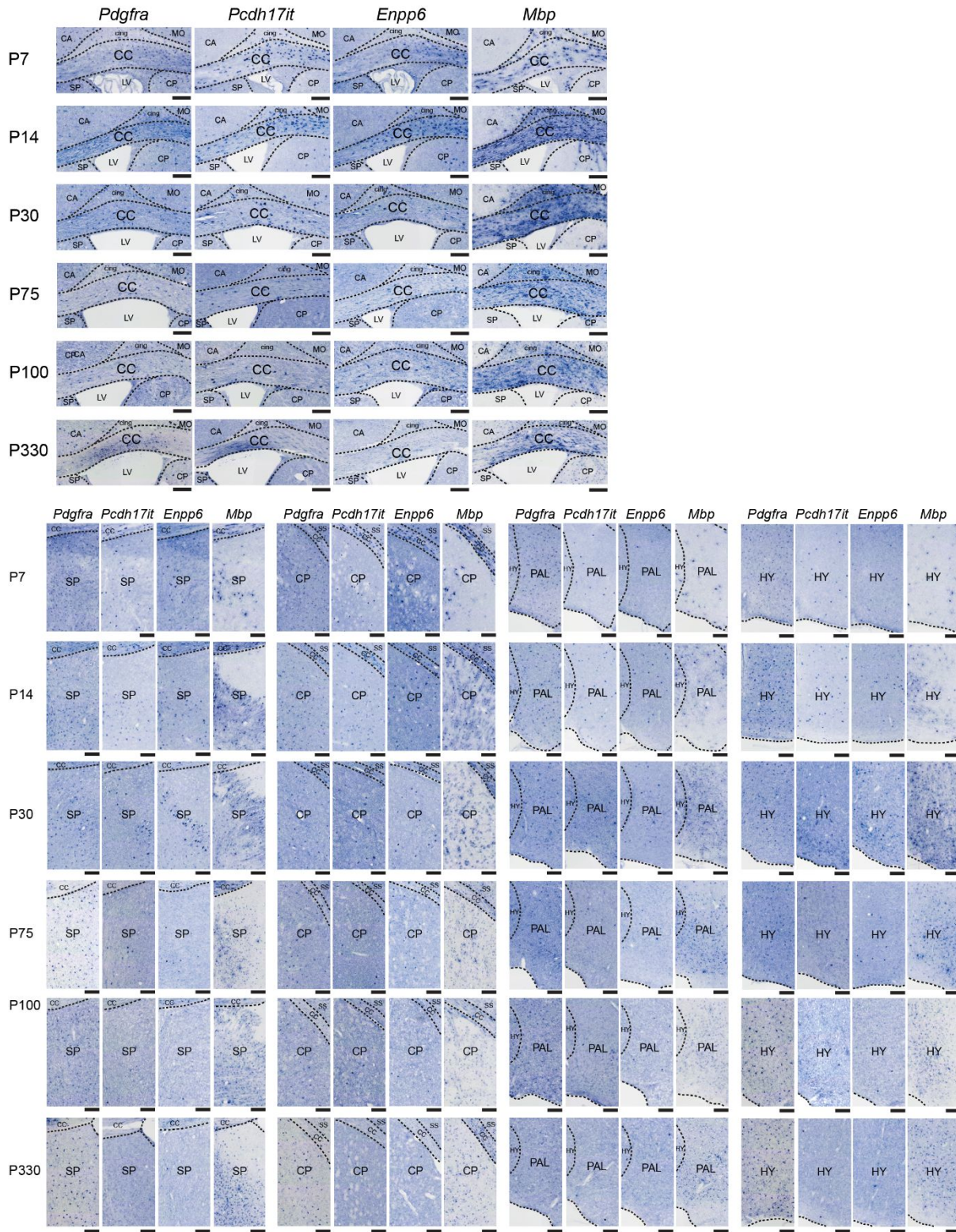
Figure_S1



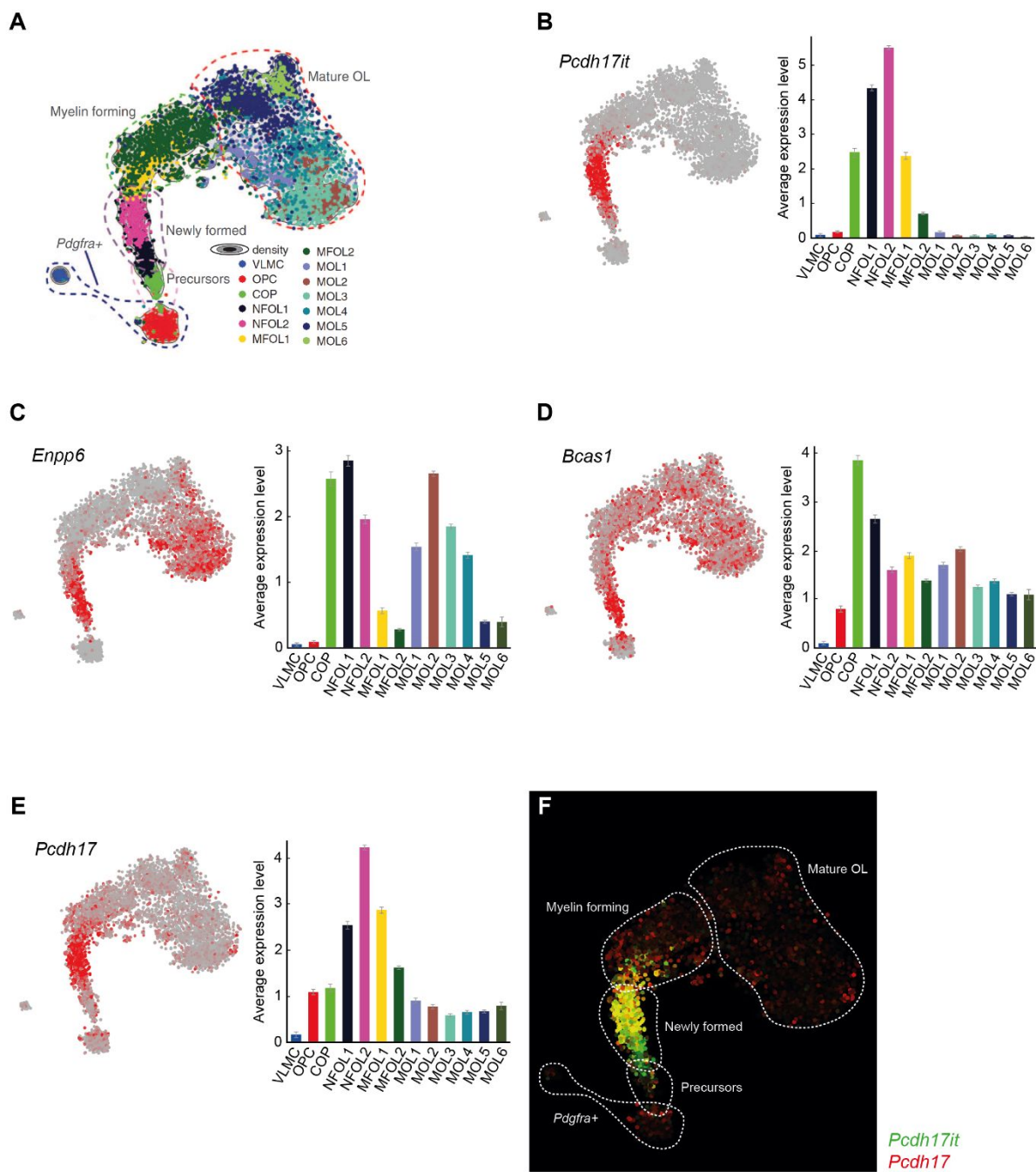
Figure_S2



Figure_S3



Figure_S4



Figure_S5

Supplementary Tables

n animals	Density (cell number/mm ²)										
E15.5 (n = 6)	NCx	CP	SVZ/VZ	PCx	Str	GE	POA				
<i>Pdgfra</i> ⁺ cell	55.48 ± 3.51	133.70 ± 8.06	55.17 ± 3.06	120.00 ± 5.88	100.60 ± 5.00	84.08 ± 2.48	97.02 ± 6.36				
<i>Pcdh17it</i> ⁺ cell	0.00 ± 0.00	0.00 ± 0.00	0.00 ± 0.00	0.00 ± 0.00	0.00 ± 0.00	0.00 ± 0.00	0.00 ± 0.00				
<i>Enpp6</i> ⁺ cell	0.00 ± 0.00	0.00 ± 0.00	0.00 ± 0.00	0.00 ± 0.00	0.00 ± 0.00	0.00 ± 0.00	0.00 ± 0.00				
<i>Mbp</i> ⁺ cell	0.00 ± 0.00	0.00 ± 0.00	0.00 ± 0.00	0.00 ± 0.00	0.00 ± 0.00	0.00 ± 0.00	0.00 ± 0.00				
P0 (n = 6)	CA	MO	SS	PIR	CC	DSVW	SP	CP	PAL	HY	
<i>Pdgfra</i> ⁺ cell	98.86 ± 7.34	144.00 ± 9.84	206.33 ± 8.77	160.55 ± 8.04	247.97 ± 4.92	205.20 ± 24.07	120.49 ± 2.88	138.24 ± 4.63	120.71 ± 1.65	152.58 ± 7.03	
<i>Pcdh17it</i> ⁺ cell	0.76 ± 0.76	0.48 ± 0.30	0.04 ± 0.03	0.30 ± 0.30	0.89 ± 0.61	6.86 ± 3.19	0.00 ± 0.00	0.00 ± 0.00	0.00 ± 0.00	0.00 ± 0.00	
<i>Enpp6</i> ⁺ cell	0.76 ± 0.76	0.48 ± 0.30	0.04 ± 0.03	0.00 ± 0.00	0.60 ± 0.60	3.92 ± 1.96	0.00 ± 0.00	0.00 ± 0.00	0.00 ± 0.00	0.00 ± 0.00	
<i>Mbp</i> ⁺ cell	0.00 ± 0.00	0.24 ± 0.24	0.02 ± 0.02	0.00 ± 0.00	0.30 ± 0.30	1.96 ± 1.24	0.00 ± 0.00	0.00 ± 0.00	0.00 ± 0.00	0.00 ± 0.00	
P7 (n = 6)	CA	MO	SS	PIR	CC	SP	CP	PAL	HY		
<i>Pdgfra</i> ⁺ cell	287.13 ± 14.76	600.18 ± 22.65	584.64 ± 15.46	371.81 ± 18.80	1129.82 ± 85.13	577.26 ± 42.88	517.32 ± 35.78	483.32 ± 18.37	417.25 ± 29.47		
<i>Pcdh17it</i> ⁺ cell	6.15 ± 1.16	5.84 ± 0.16	7.48 ± 0.65	9.52 ± 1.34	180.32 ± 11.28	13.72 ± 3.15	30.13 ± 4.34	14.34 ± 1.14	15.83 ± 2.61		
<i>Enpp6</i> ⁺ cell	5.52 ± 0.84	5.17 ± 0.70	6.33 ± 0.60	5.90 ± 0.61	157.88 ± 3.44	11.61 ± 0.98	17.28 ± 2.50	12.78 ± 0.84	9.57 ± 0.92		
<i>Mbp</i> ⁺ cell	4.24 ± 0.51	3.98 ± 0.42	5.59 ± 0.75	6.11 ± 0.58	149.31 ± 6.66	9.54 ± 0.99	16.58 ± 1.29	10.66 ± 0.93	7.78 ± 0.77		
P14 (n = 6)	CA	MO	SS	PIR	CC	SP	CP	PAL	HY		
<i>Pdgfra</i> ⁺ cell	153.00 ± 16.19	268.18 ± 22.65	308.99 ± 31.99	247.43 ± 6.44	569.01 ± 46.74	348.00 ± 24.83	317.58 ± 10.60	355.2 ± 8.99	404.46 ± 10.18		
<i>Pcdh17it</i> ⁺ cell	12.00 ± 0.82	21.28 ± 2.16	22.94 ± 0.83	14.79 ± 1.40	213.91 ± 13.63	56.95 ± 5.93	56.08 ± 5.85	54.28 ± 6.68	36.27 ± 6.07		
<i>Enpp6</i> ⁺ cell	11.03 ± 1.93	18.24 ± 1.88	21.59 ± 2.64	14.96 ± 0.69	188.81 ± 2.14	51.33 ± 5.56	49.47 ± 2.13	49.56 ± 2.79	32.35 ± 1.50		
<i>Mbp</i> ⁺ cell	10.62 ± 1.12	15.77 ± 2.24	20.68 ± 1.71	13.24 ± 1.30	182.07 ± 8.39	43.99 ± 2.77	138.1 ± 8.37	44.02 ± 1.83	25.36 ± 1.73		
P30 (n = 6)	CA	MO	SS	PIR	CC	SP	CP	PAL	HY		
<i>Pdgfra</i> ⁺ cell	142.18 ± 9.51	168.03 ± 7.82	163.47 ± 8.69	177.58 ± 14.16	326.22 ± 19.29	200.78 ± 12.81	134.93 ± 11.40	233.57 ± 20.86	237.70 ± 10.81		
<i>Pcdh17it</i> ⁺ cell	12.99 ± 1.31	12.04 ± 1.28	14.08 ± 1.09	10.22 ± 1.29	91.83 ± 12.40	14.63 ± 2.70	12.34 ± 0.60	12.93 ± 2.19	25.44 ± 4.42		
<i>Enpp6</i> ⁺ cell	25.73 ± 1.70	13.83 ± 0.83	19.8 ± 1.63	11.7 ± 0.49	98.74 ± 3.77	23.4 ± 3.86	20.30 ± 2.54	31.09 ± 4.02	25.74 ± 1.91		
<i>Mbp</i> ⁺ cell	46.84 ± 1.83	102.58 ± 3.61	157.55 ± 12.95	67.66 ± 6.87	442.99 ± 26.83	204.53 ± 15.89	253.29 ± 10.81	96.26 ± 6.76	85.98 ± 4.95		
P75 (n = 6)	CA	MO	SS	PIR	CC	SP	CP	PAL	HY		
<i>Pdgfra</i> ⁺ cell	125.39 ± 12.64	132.92 ± 7.84	131.30 ± 7.47	161.49 ± 7.17	176.60 ± 21.27	198.49 ± 7.26	132.41 ± 4.06	183.46 ± 4.62	225.13 ± 4.29		
<i>Pcdh17it</i> ⁺ cell	6.09 ± 0.93	5.84 ± 0.53	5.29 ± 0.46	5.08 ± 0.91	41.11 ± 4.61	5.21 ± 0.50	4.48 ± 0.62	7.27 ± 1.00	6.06 ± 0.92		
<i>Enpp6</i> ⁺ cell	6.38 ± 1.17	5.40 ± 0.54	7.99 ± 0.96	6.17 ± 0.38	36.44 ± 2.04	11.19 ± 2.80	6.74 ± 0.74	9.35 ± 0.54	8.33 ± 1.01		
<i>Mbp</i> ⁺ cell	205.00 ± 6.41	329.65 ± 15.81	401.19 ± 20.69	121.8 ± 7.28	1813.1 ± 45.43	583.53 ± 37.70	535.23 ± 13.79	495.1 ± 25.90	178.88 ± 8.37		
P100 (n = 4)	CA	MO	SS	PIR	CC	SP	CP	PAL	HY		
<i>Pdgfra</i> ⁺ cell	104.04 ± 4.46	123.08 ± 8.40	103.83 ± 5.33	118.87 ± 5.56	163.65 ± 12.62	123.23 ± 10.68	112.9 ± 18.46	104.07 ± 11.36	168.94 ± 19.79		
<i>Pcdh17it</i> ⁺ cell	3.12 ± 0.67	3.43 ± 1.23	3.63 ± 0.81	4.41 ± 1.20	26.36 ± 3.11	4.88 ± 1.57	3.68 ± 1.07	5.30 ± 0.89	4.82 ± 1.34		
<i>Enpp6</i> ⁺ cell	5.67 ± 0.59	4.35 ± 0.81	6.70 ± 0.88	5.06 ± 0.66	31.06 ± 5.36	8.70 ± 1.56	4.29 ± 0.79	7.03 ± 1.57	5.21 ± 0.36		
<i>Mbp</i> ⁺ cell	211.75 ± 10.30	472.6 ± 59.60	559.48 ± 28.85	152.44 ± 13.63	2065.63 ± 74.92	629.17 ± 44.47	595.9 ± 19.75	563.07 ± 48.79	233.33 ± 12.90		
P330 (n = 4)	CA	MO	SS	PIR	CC	SP	CP	PAL	HY		
<i>Pdgfra</i> ⁺ cell	102.26 ± 15.68	121.40 ± 8.36	103.07 ± 4.48	117.84 ± 14.48	155.67 ± 5.89	120.85 ± 14.08	110.18 ± 16.30	99.60 ± 16.48	154.28 ± 7.80		
<i>Pcdh17it</i> ⁺ cell	1.38 ± 0.09	1.77 ± 0.17	0.78 ± 0.10	2.70 ± 0.29	6.71 ± 1.28	1.59 ± 0.41	1.50 ± 0.52	2.40 ± 0.19	2.56 ± 1.01		
<i>Enpp6</i> ⁺ cell	3.76 ± 1.24	2.11 ± 0.50	3.42 ± 0.84	2.86 ± 0.43	11.07 ± 1.80	5.16 ± 1.90	2.12 ± 0.54	3.62 ± 0.84	3.06 ± 0.23		
<i>Mbp</i> ⁺ cell	216.82 ± 9.21	477.33 ± 17.02	562.65 ± 45.21	156.93 ± 4.11	2134.78 ± 198.10	639.42 ± 22.18	607.94 ± 26.36	565.03 ± 26.97	236.62 ± 6.88		